©2019 This manuscript version is made available under the CC-BY-NC-ND 4.0 license http://creativecommons.org/licenses/by-nc-nd/4.0/

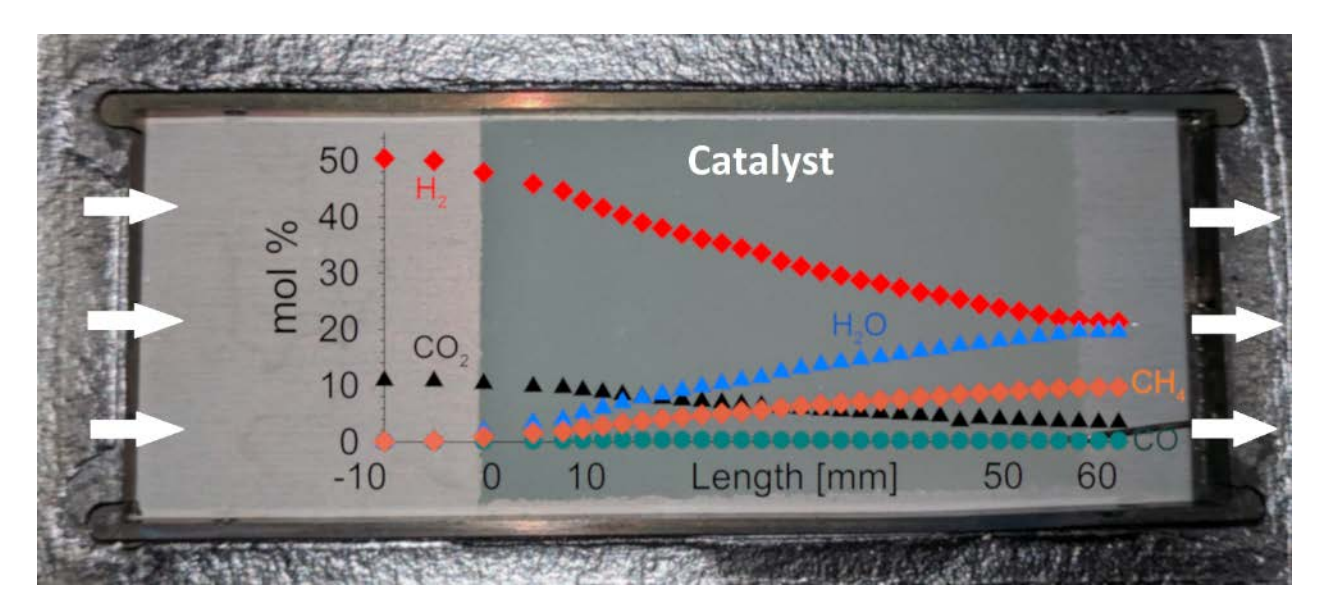
https://doi.org/10.1016/j.cej.2018.09.161

Preparation and characterization of Ni/Al₂O₃ catalyst coatings on FeCrAl-loy plates used in a catalytic channel reactor with in-situ spatial profiling to study CO₂ methanation.

Jose A. Hernandez Lalinde¹, JingSi Jiang¹, Gabriel Jai¹ and Jan Kopyscinski*¹

¹Department of Chemical Engineering, McGill University, 3610 University Street, Montreal, Canada

Graphical Abstract



Abstract

The catalyzed CO₂ methanation is an important step in the Power-to-Gas process, and obtaining accurate kinetic data for this fast and exothermic reaction is challenging. An optically accessible catalytic plate reactor with spatially-resolved measurement techniques provides the opportunity to collect high quality kinetic data for this heterogeneous system by gathering catalyst surface temperature and gas composition profiles along the reactor axis. This reactor requires a well-coated catalyst plate with an uniform and known catalyst mass distribution. Three different methods (brush, spin and frame coating) for the deposition of ready-made Ni/Al₂O₃ catalysts onto FeCrAl-

loy plates were examined. To enhance the adhesion of the catalyst, a thermal pre-treatment of the plate and the use of an alumina-based binder were needed. A homogeneous coating was achieved with frame coating, using a slurry with a total solid (i.e., catalyst and binder) to liquid ratio of $0.25:5~g_{solids}/ml_{solution}$, catalyst to binder mass ratio of 9:1 and a mixed water to isopropanol volume ratio 1:4. High resolution profilometry confirmed the homogeneity of the produced coating with a constant catalyst mass distribution of $1.5\pm0.1~mg_{cat}~mm^{-1}$. Gas composition and catalyst surface temperature profiles were acquired for the CO_2 methanation at 355 °C, 1 bar with total gas hourly space velocities of 68.5 and $103~l_N~h^{-1}~g_{cat}^{-1}$. Approximately 60 points per gas species per experiment were collected, which is a huge advantage compared to typical steady-state integral reactor with end-of-pipe measurement resulting in a single data point.

Keywords: Ni/Al₂O₃ wash-coating; spatially-resolved measurement; CO₂ methanation; kinetic measurements; IR thermography.

1 Introduction

Kinetic data for gas-solid heterogeneous catalyzed reactions are usually collected employing small laboratory fixed bed reactors in which the exit gas composition is measured only (end-of-pipe solution). Thus, a large number of experiments is required, as each experiment results in a single data point per gas species. In addition, to avoid excessive temperature changes associated with exothermic or endothermic nature of the reactions, highly diluted gas mixtures (> 90% inert gas) and/or diluted catalyst beds are used. A serious limitation of the traditional systems is the necessity to reach a gas composition at the reactor exit that is sufficiently far away from chemical equilibrium. These conditions under which the kinetic data are collected may not be industrially

relevant. Working under industrially-relevant conditions usually requires a continuous process using an integral reactor, which has significant heterogeneities such non-uniform catalyst mass distribution, concentration and temperature gradients along the axial and radial directions. Kinetic measurements (data collection) and modeling (parameter estimation and model discrimination) are difficult due to the lack of knowledge of these gradients. In-situ spatially-resolved analytical techniques in which the gas composition and catalyst surface temperature along the reactor axis are measured allow to close the knowledge gap as they combine differential and integral reactor systems and reduce the number of experiments conducted [1].

A number of techniques have been designed to provide spatially-resolved profiles of gas compositions and temperatures in different reactor configurations such as catalytic plate reactors [1–3], monolith [4–7], fluidized bed [8–10], coated metal foam [11–15] and fixed bed [16–18]. In most of these cases invasive methods using a movable capillary, thermocouple and/or pyrometer were used, while only a few studies applied non-invasive methods such as IR-thermography [1], Raman and Laser Induced Fluorescence (LIF) techniques [19].

Channel reactors have the advantages over fixed bed reactors as they have a high surface-to-volume ratio and thus and excellent heat transfer and small pressure drop. Another very important advantage of catalytic channel reactors is the ability to control the catalyst mass distribution along the reactor axis due to the coating procedure, which is paramount in quantifying/estimating kinetic parameters and in conducting a proper model discrimination of proposed reaction mechanisms. For fixed bed, coated foam and fluidized bed reactor systems the catalyst mass distribution along the reactor axis is unknown. Channel reactors are often constructed with metal or ceramic plates, namely the substrates, that are coated with catalysts chosen specifically for the chemical process involved. The incorporation of the active phase on the substrate is either done via a one-step or two-step process depending on the type of catalyst and application. In the one-step process a ready-

made catalyst (i.e., supported or unsupported) is coated directly on the substrate; while in the two-step process a high surface area support is coated first, which is subsequently impregnated with the active phase. For most applications (e.g., micro channel and monolith reactors) the two-step process is preferred as coating thicknesses of less then 5 µm are achieved [20–22].

This study aims developing a procedure to prepare a homogeneous coating for ready-made Nialumina catalysts onto FeCrAl-loy substrate plates that are used in an optically accessible channel
reactor to collect kinetic data for the CO₂ methanation reaction. The catalyzed CO₂ methanation is
an important reaction in Power-to-Gas process in which surplus electrical energy (i.e., wind energy)
is converted into a grid compatible gas via water electrolysis to produce hydrogen and subsequent
hydrogenation of captured carbon oxides to methane-rich gas [23]. The involved reactions (see eqs.
1 and 2) are catalyzed by supported Ni, Ru and Rh systems, of which the latter two noble metals
are more active [24–26]:

$$CO_2 + 4H_2 \leftrightarrow CH_4 + 2H_2O \quad \Delta H_R^o = -165 \ kJ \ mol^{-1}$$
 (1)

$$CO_2 + H_2 \leftrightarrow CO + H_2O \quad \Delta H_R^O = 41 \text{ kJ mol}^{-1}$$
 (2)

Most CO and CO₂ methanation systems utilize adiabatic fixed bed reactors with rather large catalysts in form of pellets or spheres (> 10 mm) such as the MCR-8 from Haldor Topsoe [27], METH-134 from Clariant [28] and CRG catalysts from Johnson Matthey [29]. However, the intrinsic reaction rates cannot be determined using such large particles due to mass and heat transfer effects. For that reason, a catalytic channel reactor with spatially resolved gas composition and catalyst surface measurement capability was designed that allows to collect high quality kinetic data using ready-made catalyst particles that are crushed to $20-45 \mu m$. An important requirement is a homogenously coated catalyst plate with a known coating thickness and catalyst mass

distribution. The amount of catalyst per spatial interval (i.e., between two capillary positions) must be known in order to determine the intrinsic reaction rates and corresponding kinetic parameters. This paper reports on coating procedures including thermal pre-treatment, catalyst slurry preparation and three different coating methods (brush, spin and frame) following the one-step process that uses the least amount of catalyst slurry. Dip and spray coating were not of interest as they require 10-50 times more slurry and thus to much catalyst, which might not be available. Catalyst and catalyst slurry have been analyzed via H_2 -temperature programmed reduction and N_2 adsorption/desorption techniques, while the plates and catalyst coatings have been characterized using X-Ray diffraction (XRD), Scanning Electron Microscopy (SEM), Energy-Dispersive X-ray Spectroscopy (EDX), profilometry and mechanical tests. Finally, spatially-resolved gas composition and catalyst surface temperature profiles for the best coated plate were recorder for the CO₂ methanation.

2 Experimental

A nickel-alumina catalyst, ~30 wt% NiO/Al₂O₃ (Johnson Matthey, UK) was used in this study. Based on the catalyst support material, a commercial aluminum-based binder (Sasol, Disperal P2) was chosen for improving catalyst adhesion onto the substrate. Both the catalyst and the binder were crushed and sieved into different size categories (i.e., < 20, 20 – 45, 45 – 90, and > 90 μ m). Only catalysts between 20 – 45 μ m and binder < 20 μ m were used in the coating development since a thin layer (< 50 μ m) was preferred for high catalyst utilization and reduced diffusion resistance. FeCrAl-loy sheets (Goodfellow, USA) with 1.0 mm thickness were used as the material for the substrate plates. These FeCrAl-loy sheets provided a thinner alternative to plates made from ceramics. At the same time, they have higher thermal conductivity and mechanical shock resistance.

2.1 FeCrAl-loy Plate Surface Pre-treatment

FeCrAl-loy (72.8 wt% Fe, 22.0 wt% Cr, 5.0 wt% Al, 0.1 wt% Y, and 0.1 wt% Zr) sheets were cut to a size of 4 x 10 cm to fit in the catalytic plate reactor setup. Plates were first treated in an ultrasonic bath at room temperature for 30 min, then heated in a muffle furnace (MTI, KSL-1500X) under various conditions to investigate the influence of thermal pre-treatment on the growth of alumina whiskers. Heating rate was set to $10~^{\circ}$ C min⁻¹, while the maximum temperature and soak time were varied between $800 - 1000~^{\circ}$ C and 24 - 36~h, respectively.

2.2 Slurry preparation

To obtain a mixed catalyst and binder slurry, first 5 ml of solvent (i.e., deionized water or isopropanol (99.5 %, Fisher Chemical, Canada) or a mixture of both) was prepared. Then the appropriate amount of Disperal P2 was added under constant stirring (1000 RPM). After 1 h the crushed and sieved catalyst was added, and the final slurry was stirred for another hour at 1000 RPM. In this study, the catalyst to binder weight ratio varied from 3:1 to 9:1, the water to isopropanol volume ratio varied between 0:5 to 5:0, and the total solid (i.e., catalyst and binder) to liquid ratio varied between 0.25:5 or 1.5:5 g_{solid}/ml_{solution}.

2.3 Coating procedure

Prior to the coating, the plates were weighed and the non-intended areas for coating were taped. The total coated area was 3.8 x 6 cm. Three different coating methods were investigated: (1) brush coating, (2) spin coating, and (3) frame coating (Figure 1). As mentioned earlier, other coating methods such as dip and spary coating were not of interest as they would use way more catalyst and slurrly.

In **brush coating** approximately 2 ml of coating slurry was dropped onto the uncoated area on the front side of the plate using a glass pipette. A brush was used to manually distribute the slurry onto

the center area. One gentle stroke along the length of the plate was applied to produce a visually good coating.

Spin coating was performed using a Laurell WS-650-N23 spin coater. The plate was secured by vacuum at the center of the spin coater and 1.5 – 2.5 ml of slurry were poured to the center of the coated area using a pipette. Subsequently, the spin coater was set to 100 RPM for 2 min and then to 250 RPM for 3 min. Once the slurry covered the entire coating area, the program was stopped, and the plate was air dried overnight. Faster spinning rates (500 RPM) were preliminary tested, nevertheless high rotational speed resulted in high centrifugal forces driven the slurry away (results not shown). Also, slower (50 RPM) spinning rates resulted in either incomplete coating coverage or extremely uneven coverage (results not shown).

Frame coating was done using a rectangular 3D printed frame made from polylactic acid (PLA), which was fixed on top of the heat-treated FeCrAl-loy plate (Figure 1C). The plate and frame were horizontally leveled. Then, 1.3 – 2.5 ml of slurry was poured into the framed area using a glass pipette. The total area was covered with the slurry and had a height of about 0.6 to 1.1 mm depending on the amount added.

Once the slurry covered the entire desired coating area (for each method), the plate was air dried overnight and subsequently calcined at 375 °C for 5 h in a muffle furnace. After calcination the plates were weighted to determine the total solid and catalyst loadings. Neither the slurry preparation nor the coating procedure changed the nickel loading on the catalysts.

2.4 Characterization techniques

X-ray diffraction (XRD) analyses were performed on thermally treated FeCrAl-loy plates to investigate alumina whisker growth (Bruker, D8 Discovery) with a two-dimensional VÅNTEC-

500 detector and $CuK\alpha 1$ ($\lambda = 1.54056$ Å) radiation source was used to determine crystalline structure (tube voltage 40 kV, tube current 20 mA, scan rate 5° min⁻¹).

Scanning Electron Microscopy (SEM) analyses were performed using an FEI Inspect F-50 field emission scanning electron microscope to examine the morphology of coatings and the aluminum whisker growth of the thermally treated FeCrAl-loy plates. In addition, Energy-Dispersive X-ray Spectroscopy (EDX) experiments were performed on the coating-substrate for elemental analysis and distribution. The coated plate was prepared as metallographic cross-section. The sample was embedded in an epoxy resin for the cross-section preparation and was consequently grinded using SiC sand paper from 220 to 2500 mesh. A thin 4 nm Pt film was deposited onto the cross section for improving conductivity (EM ACE600, Leica Microsystems, Austria).

Temperature programmed reduction (H₂-TPR) of the catalyst and dried slurries were carried out in fixed bed reactor setup coupled with a calibrated mass spectrometer (Hiden Analytical, HPR-20, UK). Approximately 100 mg of sample was heated under Ar atmosphere (40 ml_N min⁻¹, 99.999%, Megs) with a rate of 10 °C min⁻¹ to 310°C for 3 h to remove moisture. After cooling the sample to room temperature, H₂ (99.999%, Megs) was introduced and the sample heated at 5 °C min⁻¹ to 950 °C while recording the mass to charge ratio (m/z = 18 for H₂O) with the mass spectrometer. Flow rates of H₂ and Ar were respectively set to 10 and 40 ml_N min⁻¹ (subscript *N* denotes normal condition with T = 0 °C and p = 1 bar_{abs}).

To investigate the influence of the binder and solvent on the catalyst properties, the prepared slurries were calcined at 375 °C for 5 h and then analyzed by N₂ adsorption/desorption and H₂ uptake (Autosorb iQ, Quantachrome). N₂ adsorption/desorption measurements (-196 °C) were conducted to determine total surface area. Before the analysis, the sample was degassed under vacuum for 16 h at 200 °C. For H₂ uptake (chemisorption), approximately 100 mg of the sample

was placed in a U-shaped quartz tube, preheated in He at 310 °C with a heating rate of 5 °C min⁻¹ for 1 h, then reduced with H₂ at its optimum reduction temperature obtained from catalyst H₂-TPR for another 3 h, then evacuated for 1 h and subsequently cooled to 40 °C, where all measurements were taken at pressures ranging from 50 to 800 mbar. All surface area analyzes were conducted 3 times to assure data accuracy and reproducibility.

To determine the actual nickel loading, 10 mg of the catalyst was digested using a mixture of 2 ml of concentrated hydrochloric acid (37 wt%, Fisher Scientific) and 5 ml of concentrated nitric acid (67 wt%, Fisher Scientific) at 95 °C for 2 h. The mixture was diluted and subsequently analyzed using a TraceScan Inductively Coupled Plasma – Optical Emission Spectroscopy (ICP-OES, iCAP 6500 dual view, Thermo Scientific) system. The instrument was calibrated prior to the measurements using nickel standards diluted at 0.5 ppm, 5 ppm, and 50 ppm and the concentration of nickel in the sample was then measured at 231.6 nm wavelength, which is the characteristic wavelength of nickel.

2.5 Profilometry

Height profiles of the coated and the uncoated area were measured by profilometry (Dektak XT, Bruker, Tucson, USA). The stylus of the profilometer had a diameter of 12.5 µm and the force applied for the profilometry test was set to be 1 mg (9.8 µN) to prevent damaging the catalyst coating. The spatial resolution was set to 1 data point per 1 µm in axial direction and 1 data point every 500 µm in radial direction. By measuring the catalyst height profile of the coated area of the metal plate, the catalyst mass in the given interval, and the catalyst mass distribution was determined as described in our previous work [1].

2.6 Mechanical test

The mechanical flow tests were performed under cold flow conditions in a 3D printed channel reactor. In detail, the coated plate (calcined at 375 °C) was placed into the channel and subjected to an Ar flow of up to 600 ml_N min⁻¹ for 1 h (four times the flow rate used for activity tests). Subsequently, the weight change was recorded and the difference in the height profile along the same line was measured.

2.7 Catalytic activity and spatially-resolved tests

Figure 2 illustrates the reactor setup for catalytic activity tests. A detailed description of the setup and experimental procedure is published in our previous work [1]. In short, the setup consists of an optically accessible channel reactor in which the catalyst coated plate is placed at the bottom, while the top of the reactor is closed with a set of two quartz glass plates enabling catalyst surface temperature measurement via IR thermography (i.e., short wave infrared camera, FLIR SC2500, US). The channel itself has the dimension of 5 x 40 x 100 mm. From the side a small (0.5 mm outer diameter) movable stainless-steel capillary is introduced enabling spatially-resolved measurement of the gas composition 2 mm above the catalyst. The capillary was connected to a calibrated quadrupole mass spectrometer (Hiden Analytical, HPR-20, UK). The reactant gases were added via calibrated mass flow controllers (Voegtlin, Switzerland). Preliminary experiments have shown that neither reactant nor product gases influences in the catalyst surface measurement due to possible infrared adsorption [1].

The system was set for acquiring 60 data points along the reactor axis for each gas species and 3 data points per mm for the IR measurements (i.e., 9 data points per 1 mm² surface). Prior to the experiments, the catalyst was reduced with 20 mol% H₂ (99.999% Megs) in Ar (99.999% Megs) for 8 h at the respective reduction temperature (i.e., 490 °C), determined via H₂-TPR. The reactivity

tests were conducted at a temperature of 355 °C and 1 bar_{abs} with total volumetric flowrates of 100 or 150 ml_N·min⁻¹ at a fixed H₂/CO₂ mol ratio of 5:1 and Ar as internal standard. Prior to starting the data acquisition, the sampling orifice of the capillary was moved to the zero position, 19 mm before the coated area begins. The sampling capillary was held for 120 s at each position and moved in flow direction to the end of the reactor. Conversion of carbon dioxide (X_{CO2}) and methane selectivity (S_{CH4}) were defined per eqs. 3 to 4.

$$X_{CO_2} = \frac{\dot{n}_{CO_{2,in}} - \dot{n}_{CO_{2,out}}}{\dot{n}_{CO_{2,in}}} \tag{3}$$

$$S_{CH_4} = \frac{\dot{n}_{CH_4}}{\dot{n}_{CO_{2,in}} - \dot{n}_{CO_{2,out}}} \tag{4}$$

Only CH₄ and CO, but no C₂+ hydrocarbons were detected during all activity experiments.

3 Results and discussion

3.1 Plate thermal pre-treatment

The untreated FeCrAl-loy plate had a rather smooth surface and exhibited only diffraction pattern for FeCrAl (PDF #054-0387) as depicted in Figure 3A (XRD on the left and SEM pictures on the right). The surface consisted mainly of $10-50~\mu m$ wide valley and $10-100~\mu m$ wide hill regions (not shown).

Upon heat treatment α -Al₂O₃ like whiskers started to form. Calcined at 800 °C, the plate had visually a rougher surface than the untreated plate but exhibited only a minor diffraction peak corresponding to α -Al₂O₃ at 35° (Figure 3B). With increasing temperature to 900 °C and 1000 °C the intensity of diffraction peaks associated to α -Al₂O₃ ($2\theta = 26^{\circ}$, 35°, 42°, 58°) increased, indicating a significant growth of alumina whiskers covering the entire valley region as illustrated in the SEM as well (Figure 3C and D). A further increase of the soak time to 36 h yielded a complete

https://doi.org/10.1016/j.cej.2018.09.161

whisker growth in both valley and hill regions (Figure 3E). The increased surface roughness associated with α -Al₂O₃ formation throughout the entire surface is assumed improve coating adhesion [30,31]. If not otherwise stated, FeCrAl-loy plates were thermally treated at 1000 °C and 36 h for the remainder of the study.

3.2 Coating deposition

Table 1 summarizes the parameters for the slurry preparation as well as the achieved catalyst loadings.

Table 1. Slurry composition and solid loading for brush and spin coating experiments. W_{Cat}/W_{Binder} refers to catalyst to binder weight ratio. V_{H2O}/V_{ISO} refers to water to isopropanol volume ratio.

Slurry	Plate	Total solid [mg]	Total Liquid [ml]	W _{Cat} /W _{Bin} [g:g]	V _{H2O} /V _{ISO} [ml:ml]	Solid Loading [#] [mg]	Catalyst Loading [#] [mg]	
Brush coating								
S01	P1	1.0	5.0	9:1	5:0	7.8	7.0	
S02	P2	1.0	5.0	9:1	0:5	5.4	4.9	
S03	P3	1.0	5.0	9:1	2.5:2.5	21.6	19.4	
Spin Coating								
S04	P4	1.0	5.0	3:1	0:5	22.0	16.5	
S05	P5	1.0	5.0	3:1	4:1	25.5	19.1	
S06	P6	1.0	5.0	3:1	2.5:2.5	16.6	12.5	
S07	P7	1.0	5.0	3:1	1:4	118.2	88.7	
S08	P8	1.5	5.0	9:1	1:4	151.9	136.7	

[#] all reported loadings \pm 0.2 mg; (Solid = Catalyst + Binder)

3.2.1 Brush coating

Brush coating prepared either with pure water-based or pure alcohol-based slurry resulted in insufficient coverages of the catalyst particles (Figure 4A and B). The coating of the water-based slurry exhibited a mud-like structure, as the Disperal P2 particles disaggregated upon stirring in water to nanoparticles (~25 nm), which formed a gelatinous boehmite (aluminum oxide linked by hydrogen bonding in the form of $n[HO - Al - O] \cdot H - O - H \cdot \cdot [O - Al - OH] n$) [32,33].

Using alcohol instead of water diminished the gel-formation, however, due to fast evaporation of the solvent (alcohol) large portions of the plate were uncoated (Figure 4 B). A mixed solvent-based water and isopropanol ($V_{H2O}/V_{ISO}=1:1$) slurry, S03, yielded a better coating and catalyst loading (Figure 4C). The 3D surface profilometry for plate P3 confirmed a very thin layer of catalyst deposited over the heat-treated plate, Figure 5. The height profile showed a single layer of catalyst particles (catalyst clusters) followed by exposed areas of the plate where no particles were noticeable. The coating height measured was between 25 – 40 μ m, with no particles overlapping.

The plates coated with pure water- or isopropanol-based slurries yielded a poor loading of 7.0 and 4.9 mg for plates P1 and P2, respectively (Table 1). The plate coated with mixed slurry, P3, reached higher loadings, 19.4 mg of catalyst deposited. Even though 2 ml of slurry was used in the coating process, most of the slurry and thus catalyst stayed within the brush.

3.2.2 Spin coating

Due to the presence of "mud"-like structure in pure water-based slurries, only isopropanol-based slurry S04 and mixed solvent-based slurries, S05-S08, were prepared for spin-coating tests.

Plate P4 coated with pure isopropanol slurry S04 ($V_{H2O}/V_{ISO} = 0.5$) presented multiples zones of coated and uncoated areas (Figure 6A). A better surface coverage was achieved with the mixed

slurries, with the best result for slurry S07 (water to isopropanol ratio of 1:4, Figure 6D). The coatings consisted of mainly spherical particles that retained their original shape. However, slurry S05 resulted in a plate P5 in which a mud-like structure was formed due to the high water content. Plates 4, 5 and 6 had catalyst loadings of less than 20 mg_{cat} (Table 1). The increase in the isopropanol content for mixed-solvent slurry, S07 ($V_{H2O}/V_{ISO} = 1:4$), increased the catalyst loading more than fourfold to ~89 mg_{cat}. The coating consisted mainly of well differentiated catalyst particles with little uncoated areas, Figure 6D.

With the aim of achieving a better coverage with a higher catalyst loading, while allowing the minimum formation of the mud-like structure the total amount of solid in the slurry was increased from 1.0 g to 1.5 g. Plate P8 exhibited visually a good coating (Figure 7), with a higher catalyst loading (i.e., 136.7 mg_{cat} vs 88.7 mg_{cat} for S08 vs S07, Table 2). However, upon closer inspection the formation of multiple layers (i.e., particles overlapping) were visible, which was confirmed by profilometry as depicted in Figure 8A. A maximum coating height of 190 μ m was measured in a concentrated area were the catalyst was added during the spin-coating process. The coating height decreased radially from this area of catalyst accumulation towards the edges of the plate (e.g., 25 - 50 μ m).

Irregular coatings results in non-homogeneous catalyst mass distribution. For plate P8 the catalyst mass distribution varied between 1.2 and 4.8 mg_{cat} mm⁻¹, with the maximum loading found at around 32 mm measured along the coating length, Figure 8B. Non-homogeneous coating in form of catalyst accumulations may lead to hot-spots [34] during the activity measurement and kinetic data collection. This needs to be avoided, especially for fast and highly exothermic reactions such as the methanation of carbon oxides. Furthermore, an accurate reactor model to determine kinetic parameters requires the knowledge of the catalyst mass distribution. In detail, the catalyst mass

distribution may change along the reactor axis but is assumed to be constant perpendicular to the flow direction. Thus, spin-coating technology is not applicable to deposit the catalyst onto the plate that is used to collect high quality kinetic data.

Yet another disadvantage of spin coating was the large amount of slurry that spread beyond the desired coating area which had a rectangular shape instead of the circle.

3.2.3 Frame coating

The alcohol-based and mixed-based slurries used in the previous methods did not yield a sufficient coating (i.e., coverage, mass distribution) using the frame coating due to high amount of solid in the slurry. Thus, for this coating method the solids to liquid ratio was reduced down to 0.25 g per 5 ml liquid, while keeping the same catalyst to binder weight ratio and water to isopropanol volume ratio, 9:1 and 1:4 respectively (Table 2). Compare to brush and spin-coating, the frame coating procedure does not result in a loss of catalyst as the slurry is poured into framed area.

Table 2. Frame coating summary of slurry preparation and solid loading. W_{Cat}/W_{Bin} catalyst to binder weight ratio. V_{H2O}/V_{Iso} water to isopropanol volume ratio.

Slurry	Plate	Total solid [mg]	Total Liquid [ml]	W _{Cat} /W _{Bin} [g:g]	V _{H2O} /V _{Iso} [ml:ml]	Slurry applied [ml]	Solid Loading [mg]	Catalyst Loading [mg]
S09	P9	0.25	5	9:1	1:4	1.3	43.1	38.8
S09	P10	0.25	5	9:1	1:4	1.5	51.4	46.3
S09	P11	0.25	5	9:1	1:4	2.0	79.7	71.7
S09	P12	0.25	5	9:1	1:4	2.5	97.3	87.6

Slurry S09 allowed a better control of the catalysts deposited onto the metal substrate plates indicated by the linear relationship between the slurry applied onto the plate and the final catalyst loading (Figure 9).

A minimum of 1.3 ml, plate P9, was necessary for a visually complete coverage of the target coated area yielding a catalyst loading of approximately 39 mg_{cat}. As the amount of slurry poured onto the metal substrate increased, the catalyst loading increased linearly up to 88 mg_{cat}, plate P12.

SEM image and EDX line scan along the cross-section of a coated plate with S09 slurry is illustrated in Figure 10. The cross section shows the rough surface of the heat-treated FeCrAl-loy plate (Figure 10A). The coating morphology was characterized by single particles (~45 μm) and smaller overlapping particles (< 20 μm) maintaing a coating thickness between 30 to 60 μm. EDX line analysis was performed over a single catalyst particle, 42 μm diameter (Figure 10B). The signal strength of the main elements Fe, Cr, Al, Ni and O in the coating-substrate system showed high intensities for Fe, Cr, Al in the FeCrAl-loy plate due to the inherent composition of the plate (72.8 wt% Fe, 22.0 wt% Cr, 5.0 wt% Al) and O derived from the thermal heat treatment (i.e., calcination and post coating treatment), see Figure 10C. At the coated area the intensities for Al, Ni and O were enhanced representing the NiO/Al₂O₃ catalyst. Fe, and Cr are predominantly found in the metal substrate. Al and O are found in both, catalyst coating and metal substrate, while Ni is predominantly found in the catalyst coating (Figures 10C and 11).

A comprehensive representation of the coating for plate P12 is shown as a 3D surface profilometry and catalyst mass distribution in Figure 12A and B, respectively. The obtained coating was nearly homogeneous with a height profile between $40-60~\mu m$ in flat area. The data for the coating thickness have an estimated accuracy of \pm 10 μm due to roughness of the substrate plate and the catalyst coating itself (visualized in the side-view SEM in Figure 10A and B). At the beginning and at the end of the coated area (first 2 mm and last 2 mm) a thickness of $90-120~\mu m$ was measured indicated an accumulation of catalyst particles. This particle overlap was most likely due to the surface tension close to the frame walls, where the slurry developed a concave liquid surface.

Frame coating clearly improves the catalyst mass distribution compared to the spin and brush coating methods. The catalyst mass distribution of the frame coated plate P12 varied between 1.4 and 1.7 mg_{cat} mm⁻¹ in the flat region of the coating (2 - 56 mm length), and a maximum of 2.3 and $2.8 \text{ mg}_{cat} \text{ mm}^{-1}$ was found at the highest measured areas (first 2 mm and last 2 mm unit length).

The best coating results in terms of homogeneous catalyst mass distribution were achieved with frame coating. For further analyses such as mechanical tests, slurry characterization and activity tests only frame coated plates were used.

The mechanical tests were conducted only on these plates with three different parameters. (1) A

3.3 Mechanical test

thermally untreated FeCrAl-loy plate was coated with slurry S09, but without the addition of a binder. (2) FeCrAl-loy plate was heat treated at 800 °C for 24 h and coated with slurry S09, without the addition of a binder. (3) FeCrAl-loy plate was heat treated at 1000 °C for 24 h and coated with slurry S09 including the binder, reduced under H₂ at 490 °C for 8 h and tested under methanation conditions at 350 °C for 4 h. The results of mechanical tests confirmed the necessity of binder addition and heat pre-treatment for FeCrAl-loy plates, to ensure good coating adhesion (Figure 13). For the first plate a weight loss of 2 wt% was measured. The photos and the height profile clearly show the loss of catalyst (Figure 13A). Heat pre-treatment of FeCrAl-loy plates at 800 °C for 24 h improved the adhesion. But still 1.3 wt % of the catalyst coated was lost (Figure 13B). Best results were observed for the plate pretreated at 1000 °C for 24 h, and coated with slurry S09 (binder added); here the catalyst weight loss was negligible and the height profile remained the same even after catalyst reduction and reactivity measurements (Figure 13C bottom). Figure 13C top illustrates a qualitative IR emissions profile during CO₂ methanation at 350 °C, while the picture in the middle shows the coated plate after the reactivity tests. Upon catalyst reduction the color changed from grey-brown to black. The reason for the very good adhesion is formation of alumina whiskers (see Figure 3E) at $1000\,^{\circ}$ C. The noise of the measured height signal is attributed to surface roughness of the substrate and coating itself as the size of the catalyst used ranged from 20 to 45 μ m.

3.4 Catalyst and slurry characterization

Frame coating method produced suitable coatings that can be used for activity experiments. Plate P12 with slurry S09 was used for the CO₂ methanation experiment. Prior to the catalytic activity tests, the influence of the slurry preparation on the catalyst properties was studied.

Temperature programmed reduction (H_2 -TPR) was used to investigate the influence of binder addition on the slurry and to determine the reduction temperature of the catalyst coating. The slurry preparation affects slightly the TPR results with respect to the fresh catalyst, Figure 14A. The fresh catalyst and the dried slurry had similar catalyst TPR characteristics. From 200 °C to 300 °C the first H_2O peaks were observed corresponding to weak NiO interactions, whereas the reduction peaks for strong NiO interactions were detected at 457 °C and 491 °C for fresh and dried slurry, respectively. N_2 adsorption/desorption curves of fresh catalyst and slurry showed a type-IV isotherm with H1 hysteresis loop, indicating the presence of mesoporous structure (pores 2 – 50 nm), Figure 14B. The slurry preparation did not change the mesoporous structure. Interestingly, the slurry exhibited a bimodal pore size distribution, Figure 14C. The first peak at a pore size of 5 nm correspond to the binder [35] that where partialy deposited within the catalyst pores which had a pore size of 10-50 nm.

Table 3 summarizes the adsorption-desorption results for catalyst and dried slurry. Nickel loadings were calculated based on dilution ratios and the initial mass of the catalyst used in the analysis.

Actual nickel oxide loadings were calculated from the measured nickel loading assuming all nickel in the catalyst exists as nickel oxide with a stoichiometric molar ratio of Ni:O = 1:1.

Table 3. Sample overview for fresh catalyst: Ni-NiO loading, N_2 adsorption/desorption results (total area, average pore size, pore volume) and H_2 -uptake.

Sample	Ni ^a [wt%]	NiO ^a [wt%]	S_{BET}^{b} $[m^2g^{-1}]$	D _{Pore} ^c [nm]	V_{Pore}^{d} [cm 3 g $^{-1}$]	H ₂ -uptake [µmol g ⁻¹]
Fresh catalyst	23.5	29.9	90	21	0.48	135
Slurry S09	21.3		95	21	0.42	125

^a Nickel content determined via ICP; ^b S_{BET} = BET total specific surface area obtained from adsorption data in the p/p^0 range from 0.05-0.25; all reported data are within ± 4 m² g⁻¹ based on repeated analysis; ^c D_{Pore} = average pore diameters calculated using Barrett-Joyner-Halenda (BJH) method; ^d V_{Pore} = pore volume was obtained at $p/p^0 = 0.97$.

The total BET surface area for the fresh catalyst was 90 ± 4 m² g⁻¹. After preparing the slurry, the total surface area was slightly increased, 95 ± 4 m² g⁻¹. The small increase in the surface area corresponds addition of binder [35].

The volumetric hydrogen uptake (chemisorption) for the fresh catalyst was 135 μ mol g_{cat}⁻¹, and combining with the elemental nickel loadings estimated from ICP (23.5 \pm 2.1 wt%) the average crystallite size was determined to be 8.1 \pm 0.1 nm (hemi-spherical Ni crystallite) with a metal dispersion of 13.0 %. The results indicated that after the catalyst slurry preparation the H₂-uptake and thus metal dispersion decreased to 125 μ mol g_{solid}⁻¹ and 10.6 %, respectively. This confirms that part of the dissolved binder covers some active nickel clusters in the porous catalyst structure, which can explain the higher reduction temperature observed with H₂-TPR (Figure 14 A). Kinetic modeling must take this effect into account.

3.5 Catalytic activity test and spatially resolved measurement

Figure 15A and B illustrates the catalyst surface temperature and gas composition profiles at the center-line for the CO₂ methanation over commercial catalyst coated on plate P12 at 355°C with a total flow rate of 100 and 150 ml_N min⁻¹, respectively. The coating starts at 0 mm and ends at 60 mm with a total catalyst loading of 87.6 mg, resulting in a total gas hourly space velocity of 68.5 and $103 \, l_N \, h^{-1} \, g_{cat}^{-1}$. More than 700 high quality kinetic data points (temperature and gas composition; 60 points per gas species) were acquired after two experimental runs. Before the coating starts, the gas composition remained constant indicating no reaction. The slight decrease in the H₂ and CO concentration (i.e., -10 to 0 mm) can be attributed to axial dispersion. Once, the coating begins CO₂ and H₂ were converted predominately to CH₄ and H₂O with only a little CO. The gas composition profiles illustrate nicely the steady decrease of the reactants and increase of the products. For both experiments the gas composition and surface temperature profiles looked similar. As expected a slightly higher initial rate and total CO₂ conversion was observed for experiments with the lower GHSV than for experiments with the higher GHSV (i.e., $X_{CO2} = 77.6\%$ vs. $X_{CO2} = 73.0\%$). Whereas the CH₄ selectivity was about the same $S_{CH4} = 98.1 \pm 1\%$ for both run. The total C, H and O balance was closed within \pm 3%. Packed bed reactor experiments with end-of-pipe measurement under the same operating conditions were conducted. In detail, fresh catalyst and the dried slurry S09 were tested and achieved CO₂ conversions of 84.6% and 83.7%, respectively, with 98% CH₄ selectivity for both catalysts. As expected the CO₂ conversion in catalytic plate reactor was slightly smaller ($X_{CO2} = 77.6\%$) due to the different flow field in which gas transfer from the bulk phase to the catalyst and vice-versa relies on diffusion perpendicular to the flow direction.

Experiments in packed bed reactor did not allow to determine high resolution temperature profiles; thus, the exact surface temperatures remain unknown. For the plate reactor, however, the temperature profiles for both runs indicate an almost isothermal behavior along the catalyst plate. The temperature difference (i.e., without and with reactive gas) was between 0 and 1 °C. Theoretical calculations show that the measured gas composition profiles approached almost chemical equilibrium at the end of the plate. At equilibrium the composition would be Ar = 49.82 mol%; $H_2 = 13.17$ mol%; $CO_2 = 0.17$ mol%; $CH_4 = 12.28$ mol% and $H_2O = 24.56$ mol%. Based on equilibrium 47 ppmV of CO should be produced; however, the concentration profiles showed at first an increase of CO in the first 10 - 15 mm, which then passed through a maximum (~3000 – 4000 ppmV) and then decreased again. The increase of CO is caused by the reversed water gas shift reaction ($CO_2 + H_2 \rightarrow CO + H_2O$); while the decrease is due to CO methanation. This behaviour would be impossible to observe in traditional packed bed reactors with exit gas measurement only. Furthermore, reaching equilibrium at the reactor outlet with our setup is not a limitation for kinetic data collection.

The IR thermography shows an even catalyst surface temperature distribution along the coated area, which confirms a homogeneous catalyst coating (Figure 16). At the side of the plate the surface temperature was a bit lower than in the center due to possible conductive heat losses at the wall. The dashed line shows the position of the IR emissions lines that were recorded for the determination of the temperature difference line profile, Figure 15A and B top.

As stated above, axial dispersion affects the gas composition profile due to low gas velocity. Both cases resulted in laminar regime. For case A with a total flow of 100 ml_N min⁻¹: $Re_{max} \sim 13$ and $v_{max} \sim 1.1$ cm s⁻¹; and for case B with a total flow of 150 ml_N min⁻¹: $Re_{max} \sim 20$ and $v_{max} \sim 1.6$ cm

s⁻¹ were calculated. Therefore, it is paramount to include axial dispersion in the reactor model that is used to conduct kinetic parameter estimation and model discrimination.

4 Conclusions

A commercial nickel catalyst $(20-45 \mu m)$ and an aluminum-based binder $(<20 \mu m)$ were used to produce a homogeneous coating onto FeCrAl-loy plates. Thermal pre-treatment of the plates at 1000 °C for at least 24 h was necessary to allow the uniform growth of aluminum oxide whiskers that improve catalyst coating adherence. Different solvent-based slurries: (a) pure DI water, (b) pure isopropanol or (c) mixed DI water-isopropanol were used with three different coating methods: (I) brush, (II) spin and (III) frame coating. Slurries prepared with pure DI water or isopropanol solvents were found to produce coatings with poor catalyst coverage. Best results in terms of homogeneous catalyst mass distribution and total loading were obtained using the frame coating technology and a slurry containing water and isopropanol with a volume ratio of 1 to 4, catalyst and binder with weight ratio of 9 to 1, and a total solid to liquid ratio of 0.25 g to 5 ml. Moreover, a minimum of slurry was used and no catalyst was lost during the frame coating. The coating preparation did not affect significantly the catalyst properties. During the spatially-resolved measurement 60 data points per gas species and catalyst surface temperature data with a resolution of 9 points per mm² per experimental run were collected. CO₂ methanation experiments conducted at 350 °C and 1 bar_{abs} with total gas hourly space velocities of 68.5 and 103 l_N h⁻¹ g_{cat}⁻¹ achieved a total CO₂ conversion of 77.6% and 73.0%, respectively, with a 98 % CH₄ selectivity.

https://doi.org/10.1016/j.cej.2018.09.161

Acknowledgements

The authors thank David Wails (Johnson Matthey, UK) for providing the nickel alumina catalyst. In addition, the authors thank F. Caporuscio, L. Cousmich, A. Golsztajn, G. Lepkyj and R. Roy for technical assistance. Financial support from the Natural Sciences and Engineering Research Council (NSERC RGPIN/04685-2014) for this study is also recognized.

References

- [1] J.H. Lalinde, K. Kofler, X. Huang, J. Kopyscinski, Improved Kinetic Data Acquisition Using An Optically Accessible Catalytic Plate Reactor with Spatially-Resolved Measurement Techniques. Case of Study: CO₂ Methanation, Catalysts. 8 (2018) 86.
- [2] M. Bosco, F. Vogel, Optically accessible channel reactor for the kinetic investigation of hydrocarbon reforming reactions, Catal. Today. 116 (2006) 348–353.
- [3] J. Kopyscinski, T.J. Schildhauer, F. Vogel, S.M.A. Biollaz, A. Wokaun, Applying spatially resolved concentration and temperature measurements in a catalytic plate reactor for the kinetic study of CO methanation, J. Catal. 271 (2010) 262–279.
- [4] O. Shakir, A. Yezerets, N.W. Currier, W.S. Epling, Spatially resolving concentration and temperature gradients during the oxidation of propylene on Pt/Al₂O₃, Appl. Catal. A Gen. 365 (2009) 301–308.
- [5] M. Hettel, C. Diehm, B. Torkashvand, O. Deutschmann, Critical evaluation of in situ probe techniques for catalytic honeycomb monoliths, Catal. Today. 216 (2013) 2–10.
- [6] J. Sa, D.L.A. Fernandes, F. Aiouache, A. Goguet, C. Hardacre, D. Lundie, et al., SpaciMS: spatial and temporal operando resolution of reactions within catalytic monoliths, Analyst. 135 (2010) 2260–2272.
- [7] J.-S. Choi, W.P. Partridge, C.S. Daw, Spatially resolved in situ measurements of transient species breakthrough during cyclic, low-temperature regeneration of a monolithic Pt/K/Al2O3 NOx storage-reduction catalyst, Appl. Catal., A. 293 (2005) 24–40.
- [8] J. Kopyscinski, T.J. Schildhauer, S.M.A. Biollaz, Methanation in a fluidized bed reactor with high initial CO partial pressure: Part I—Experimental investigation of hydrodynamics,

- mass transfer effects, and carbon deposition, Chem. Eng. Sci. 66 (2011) 924–934.
- [9] J. Kopyscinski, T.J. Schildhauer, S.M.A. Biollaz, Methanation in a fluidized bed reactor with high initial CO partial pressure: Part II— Modeling and sensitivity study, Chem. Eng. Sci. 66 (2011) 1612–1621.
- [10] J. Kopyscinski, T.J. Schildhauer, S.M.A. Biollaz, Fluidized-Bed Methanation: Interaction between Kinetics and Mass Transfer, Ind. Eng. Chem. Res. 50 (2011) 2781–2790.
- [11] R. Horn, N.J. Degenstein, K.A. Williams, L.D. Schmidt, Spatial and temporal profiles in millisecond partial oxidation processes, Catal. Letters. 110 (2006) 169–178.
- [12] R. Horn, K.A. Williams, N.J. Degenstein, A. Bitsch-Larsen, D. Dalle Nogare, S.A. Tupy, et al., Methane catalytic partial oxidation on autothermal Rh and Pt foam catalysts: Oxidation and reforming zones, transport effects, and approach to thermodynamic equilibrium, J. Catal. 249 (2007) 380–393.
- [13] R. Horn, K.A. Williams, N.J. Degenstein, L.D. Schmidt, Mechanism of H₂ and CO formation in the catalytic partial oxidation of CH₄ on Rh probed by steady-state spatial profiles and spatially resolved transients, Chem. Eng. Sci. 62 (2007) 1298–1307.
- [14] O. Korup, S. Mavlyankariev, M. Geske, C.F. Goldsmith, R. Horn, Measurement and analysis of spatial reactor profiles in high temperature catalysis research, Chem. Eng. Process. Process Intensif. 50 (2011) 998–1009.
- [15] O. Korup, C.F. Goldsmith, G. Weinberg, M. Geske, T. Kandemir, R. Schlagl, et al., Catalytic partial oxidation of methane on platinum investigated by spatial reactor profiles, spatially resolved spectroscopy, and microkinetic modeling, J. Catal. 297 (2013) 1–16.
- [16] D. Weber, D.J. Holland, L.F. Gladden, Spatially and chemically resolved measurement of

- intra- and inter-particle molecular diffusion in a fixed-bed reactor, Appl. Catal. A Gen. 392 (2011) 192–198.
- [17] J. Touitou, K. Morgan, R. Burch, C. Hardacre, A. Goguet, An in situ spatially resolved method to probe gas phase reactions through a fixed bed catalyst, Catal. Sci. Technol. 2 (2012) 1811.
- [18] J. Touitou, R. Burch, C. Hardacre, C. McManus, K. Morgan, J. Sá, et al., An in situ spatially resolved analytical technique to simultaneously probe gas phase reactions and temperature within the packed bed of a plug flow reactor., Analyst. 138 (2013) 2858–62.
- [19] J. Mantzaras, R. Bombach, R. Schaeren, Hetero-/homogeneous combustion of hydrogen/air mixtures over platinum at pressures up to 10bar, Proc. Combust. Inst. 32 (2009) 1937–1945.
- [20] O. Görke, P. Pfeifer, K. Schubert, Highly selective methanation by the use of a microchannel reactor, Catal. Today. 110 (2005) 132–139.
- [21] X. Yu, W. Yu, H. Li, S.-T. Tu, Y.-F. Han, Preparation, characterization and application of K-PtCo/Al₂O₃ catalyst coatings for preferential CO oxidation, Appl. Catal. B Environ. 140-141 (2013) 588–597.
- [22] T. Giornelli, A. Löfberg, E. Bordes-Richard, Preparation and characterization of VO_x/TiO₂ catalytic coatings on stainless steel plates for structured catalytic reactors, Appl. Catal., A. 305 (2006) 197–203.
- [23] I. Wender, Reactions of synthesis gas, Fuel Process. Technol. 48 (1996) 189–297.
- [24] G. Weatherbee, Hydrogenation of CO₂ on group VIII metals II. Kinetics and mechanism of CO₂ hydrogenation on nickel, J. Catal. 77 (1982) 460–472.

- [25] G. Weatherbee, Hydrogenation of CO₂ on group VIII metals I. Specific activity of Ni/SiO₂,
 J. Catal. 68 (1981) 67–76.
- [26] J.H. Chiang, J.R. Hopper, Kinetics of the hydrogenation of carbon dioxide over supported nickel, Ind. Eng. Chem. Prod. Res. Dev. 22 (1983) 225–228..
- [27] Haldor Topsoe, MCR-8 SNG methantion catalyst, (2018).
 https://www.topsoe.com/products/catalysts/mcr-8 (accessed August 1, 2018).
- [28] Clariant, Catalysts for Syngas, (2010). www.clariant.com (accessed August 1, 2018).
- [29] Johnson Matthey, CRG methanation catalyst, (2018). http://www.jmprotech.com/crg-methanation-catalysts-for-sng-production (accessed August 1, 2018).
- [30] J. Camra, E. Bielańska, A. Bernasik, K. Kowalski, M. Zimowska, A. Białas, et al., Role of Al segregation and high affinity to oxygen in formation of adhesive alumina layers on FeCr alloy support, Catal. Today. 105 (2005) 629–633.
- [31] P. Avila, M. Montes, E.E. Miró, Monolithic reactors for environmental applications, Chem. Eng. J. 109 (2005) 11–36.
- [32] C. Legros, C. Carry, P. Bowen, H. Hofmann, Sintering of a transition alumina: effects of phase transformation, powder characteristics and thermal cycle, J. Eur. Ceram. Soc. 19 (1999) 1967–1978.
- [33] M.C. Wefers K, Oxides and hydroxides of aluminum, Alcoa Tech, Aluminum Company of America, Pittsburgh, 1987.
- [34] M. Zanfir, A. Gavriilidis, Modelling of a catalytic plate reactor for dehydrogenation—combustion coupling, Chem. Eng. Sci. 56 (2001) 2671–2683.

https://doi.org/10.1016/j.cej.2018.09.161

[35] DISPERAL® High purity dispersible aluminas., http://www.sasoltechdata.com (accessed April 20, 2018).

List of Figures

- Figure 1 Simplified scheme of (A) brush coating, (B) spin coating and (C) frame coating.
- Figure 2 Simplified P&ID for the catalytic plate reactor system. FeCrAl-loy plate is coated with commercial Ni-alumina catalyst ($d_P = 20 45 \mu m$).
- Figure 3 XRD patterns and SEM pictures of (A) untreated and heat treated FeCrAl-loy plates at (B) 800 °C for 24 h, (C) 900 °C for 24 h, (D) 1000 °C for 24 h and (E) 1000 °C for 36 h. Reference pattern for (●) Fe-Cr-Al-loy and (▼) α-Al₂O₃ are PDF #054-0387 and #005-0712, respectively.
- Figure 4 Brush coating results: Influence of the water to isopropanol volume ratio on the coating and surface coverage for (A) slurry S01 with 5:0, (B) S02 with 0:5 and (C) S03 with 1:1. The catalyst to binder weight ratio was fixed at 9.
- Figure 5 Brush coating results: Catalyst height-profile for plate P3. ($V_{H2O}/V_{ISO} = 1:1$, $W_{Cat}/W_{Binder} = 9:1$). Total catalyst loading: 19.4 mg.
- Figure 6 Spin coating results: Influence of the water to isopropanol volume ratio on the coating and surface coverage for (A) slurry S04 with 0:5, (B) S05 with 4:1, (C) S06 with 1:1, and (D) S07 with 1:4. The catalyst to binder weight ratio was fixed at 3.
- Figure 7 SEM images of Plate P8. FeCrAl-loy coated with NiO catalyst (29.8 wt%) using spin coating. $V_{\rm H2O}/V_{\rm Iso} = 1.4 \text{ and with } W_{\rm Cat}/W_{\rm Bin} = 9.1. \text{ Total catalyst loading: } 136.7 \text{ mg.}$
- Figure 8 (A) 3D catalyst height-profile and (B) catalyst mass distribution of plate P8 produced by spin coating with $V_{\rm H2O}/V_{\rm Iso}=1:4$, $W_{\rm Cat}/W_{\rm Bin}=9:1$. Total catalyst loading: 136.7 mg.
- Figure 9 Frame coating results: Catalyst loadings achieved with frame coating for different amounts of slurry applied. S09 with $V_{H2O}/V_{Iso} = 1:4$, $W_{Cat}/W_{Bin} = 9:1$ for plates P9, P10, P11 and P12.
- Figure 10 Frame coating results with slurry S09. (A) SEM of coating cross section (B) EDS line scanning location and (C) elemental profile (Fe, Cr, Al, Ni and O) along the line.

https://doi.org/10.1016/j.cej.2018.09.161

- Figure 11 Frame coating results with slurry S09. EDS elemental mapping (Fe, Cr, Al, Ni and O). Top left merged scans.
- Figure 12 (A) 3D catalyst height-profile, and (B) catalyst mass distribution of plate P12 produced by frame coating with $V_{\rm H2O}/V_{\rm Iso} = 1:4$, $W_{\rm Cat}/W_{\rm Bin} = 9:1$. Total catalyst loading: 87.6 mg.
- Figure 13 Mechanical test results for frame coating with slurry S09. (A) untreated plate, no binder added, coating calcined at 375 °C, (B) plate calcined at 800 °C for 24 h, no binder added, coating calcined at 375 °C and (C) plate calcined at 1000 °C for 24 h, binder added, coated plated calcined at 375 °C, reduced under H₂ at 490 °C for 8 h and tested under methanation conditions at 350 °C for 4 h.
- Figure 14 (A) H₂-TPR, (B) N₂ adsorption/desorption isotherms and (C) pore size distribution results for fresh catalyst and dried slurry, S09, prepared with mixed solvent.
- Figure 15 Measured axial gas composition profiles and catalyst surface temperature difference during CO_2 methanation with $H_2/CO_2 = 5$ at 355 °C, 1 bar and a total flow rate of (A) ml_N min⁻¹ and (B) 150 ml_N min⁻¹. Plate 12 with catalyst slurry S09. Catalyst loading 87.6 mg. The dashed lines indicate the beginning and the end of the coated area. (×) temperature, (•) H_2 , (•) Ar, (•) CH_4 , (•) CO_2 , (•) H_2O , and (•) CO_2 for visualization, gas composition data for every 2 mm are shown.
- Figure 16 3D surface temperatures profile obtained during the CO₂ methanation at a set temperature of 355°C with an inlet flow rate of 150 ml_N min⁻¹, H₂:CO₂=5:1. Plate 12 with catalyst slurry S09. Catalyst loading 87.6 mg.

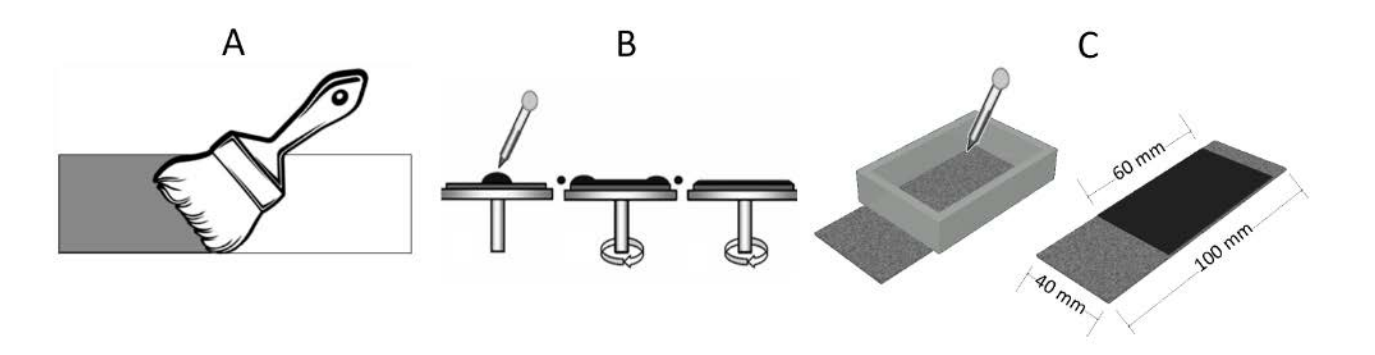


Figure 1

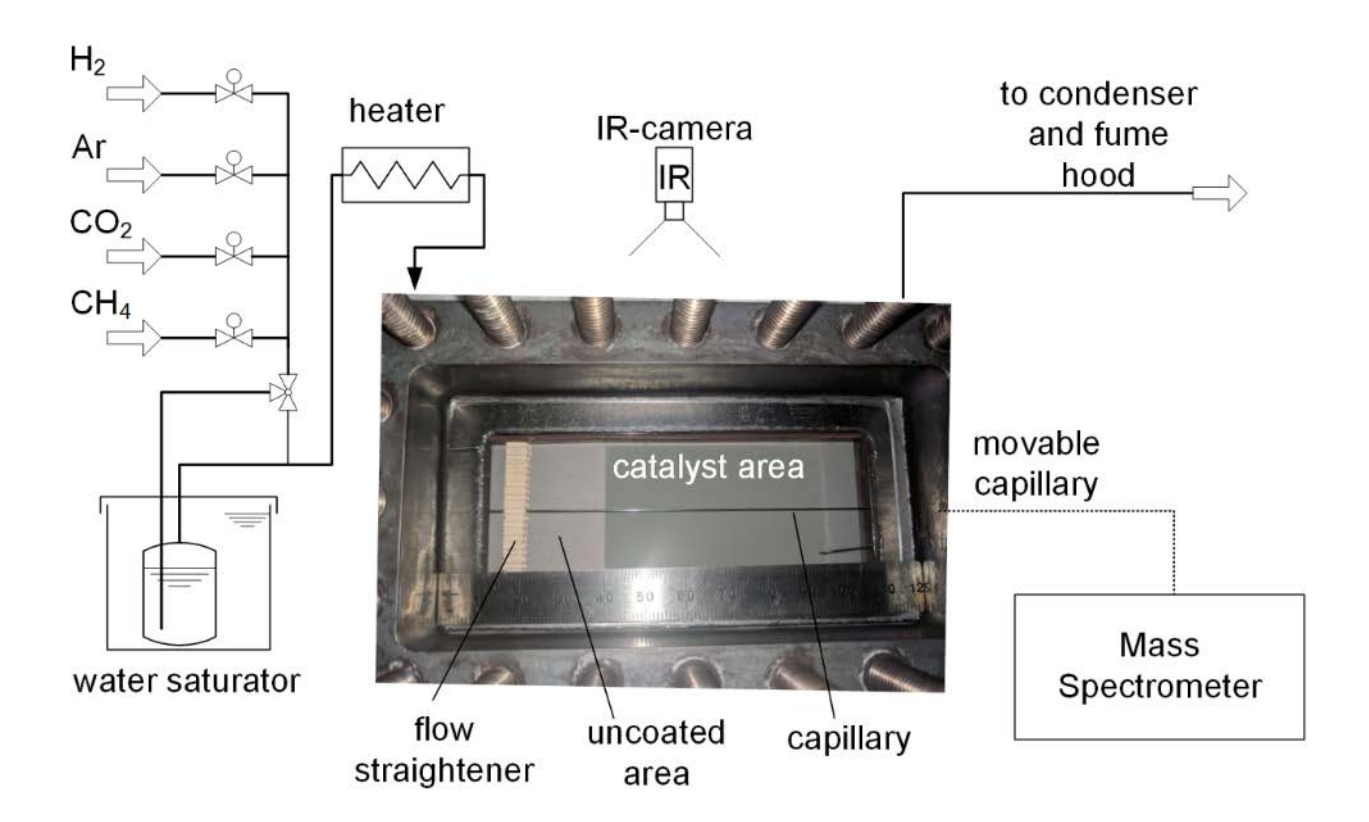


Figure 2

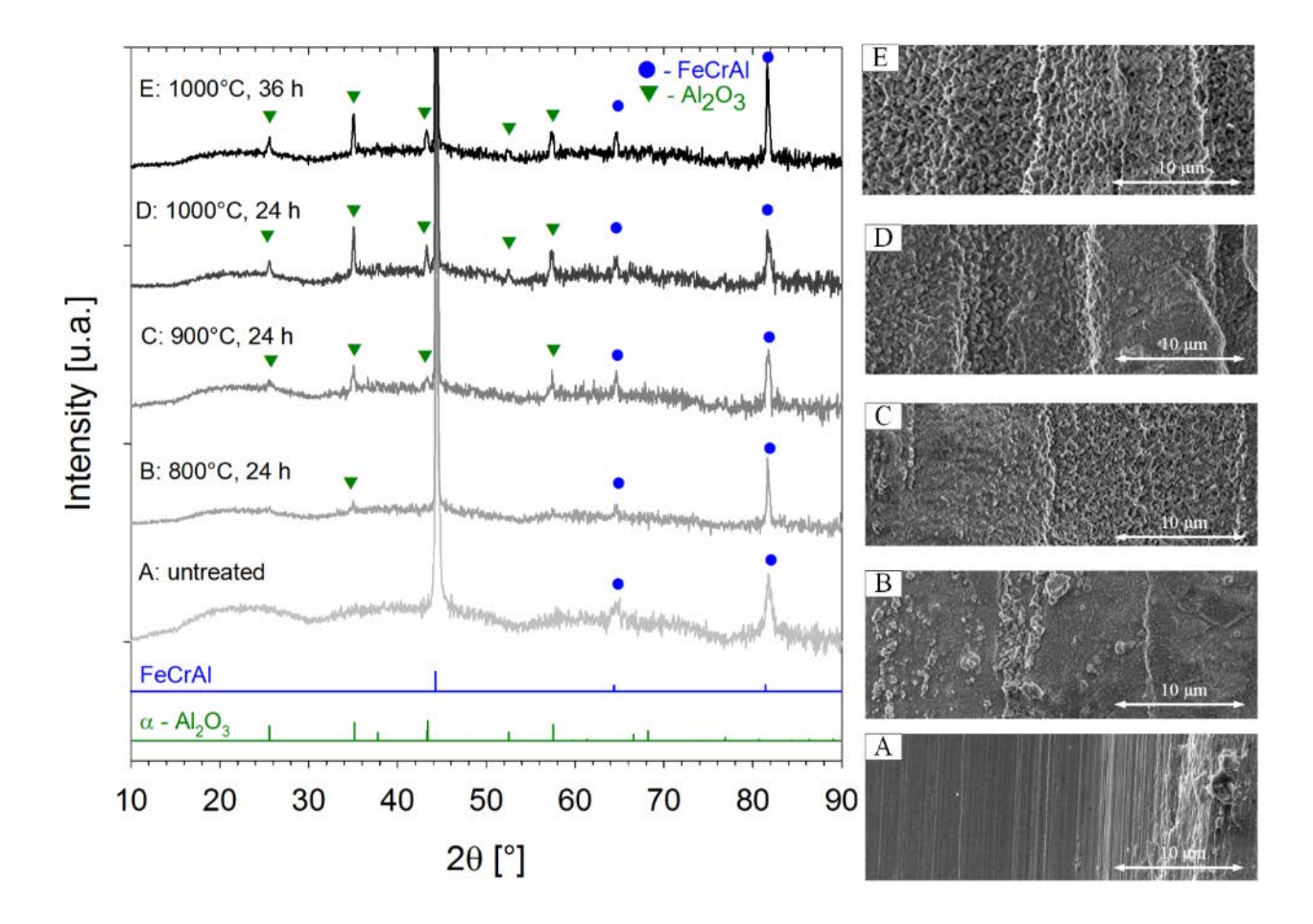


Figure 3

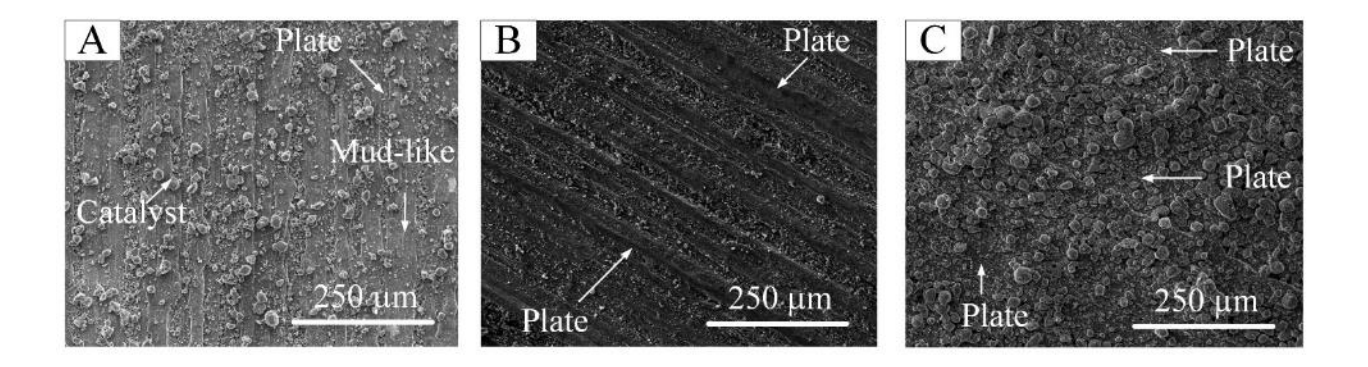


Figure 4

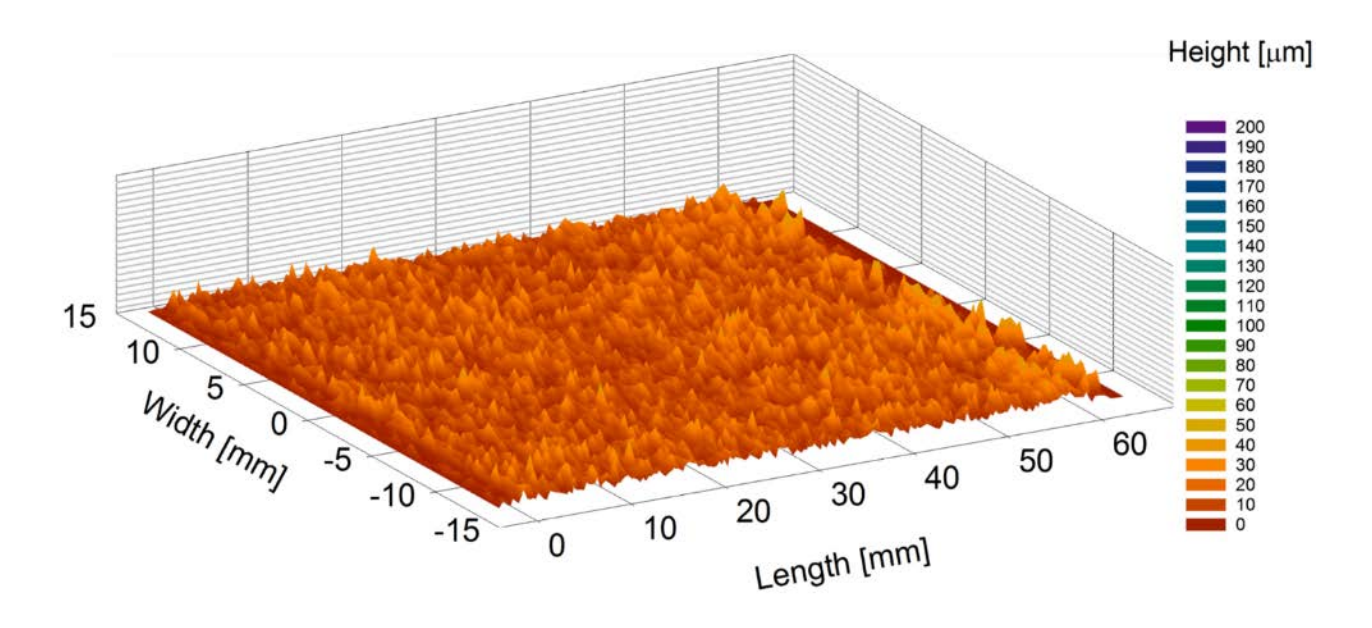


Figure 5

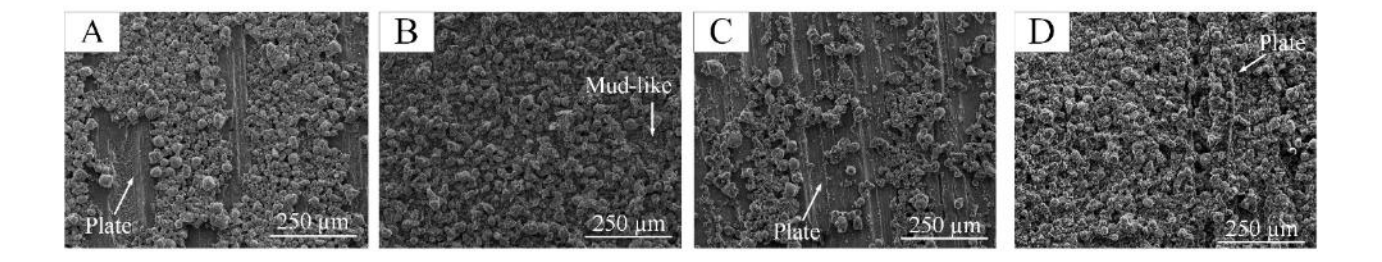


Figure 6

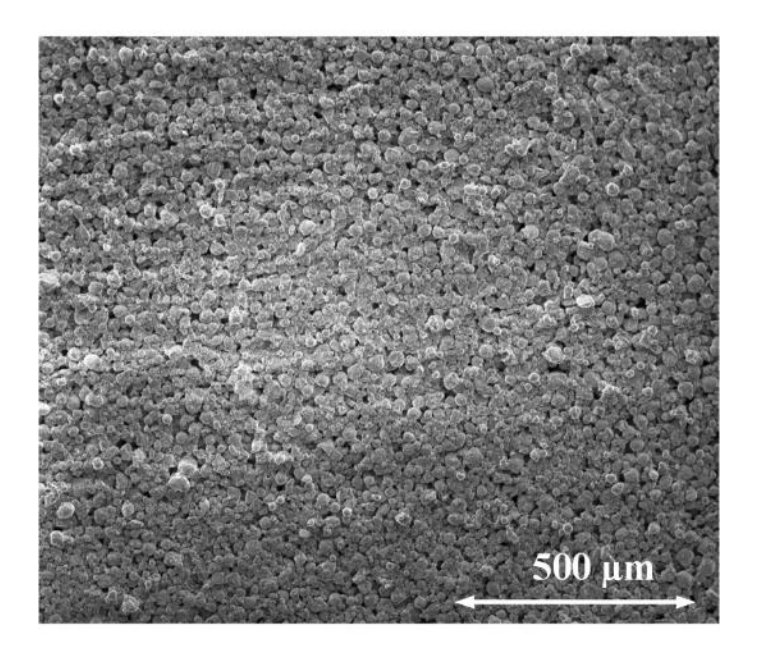


Figure 7

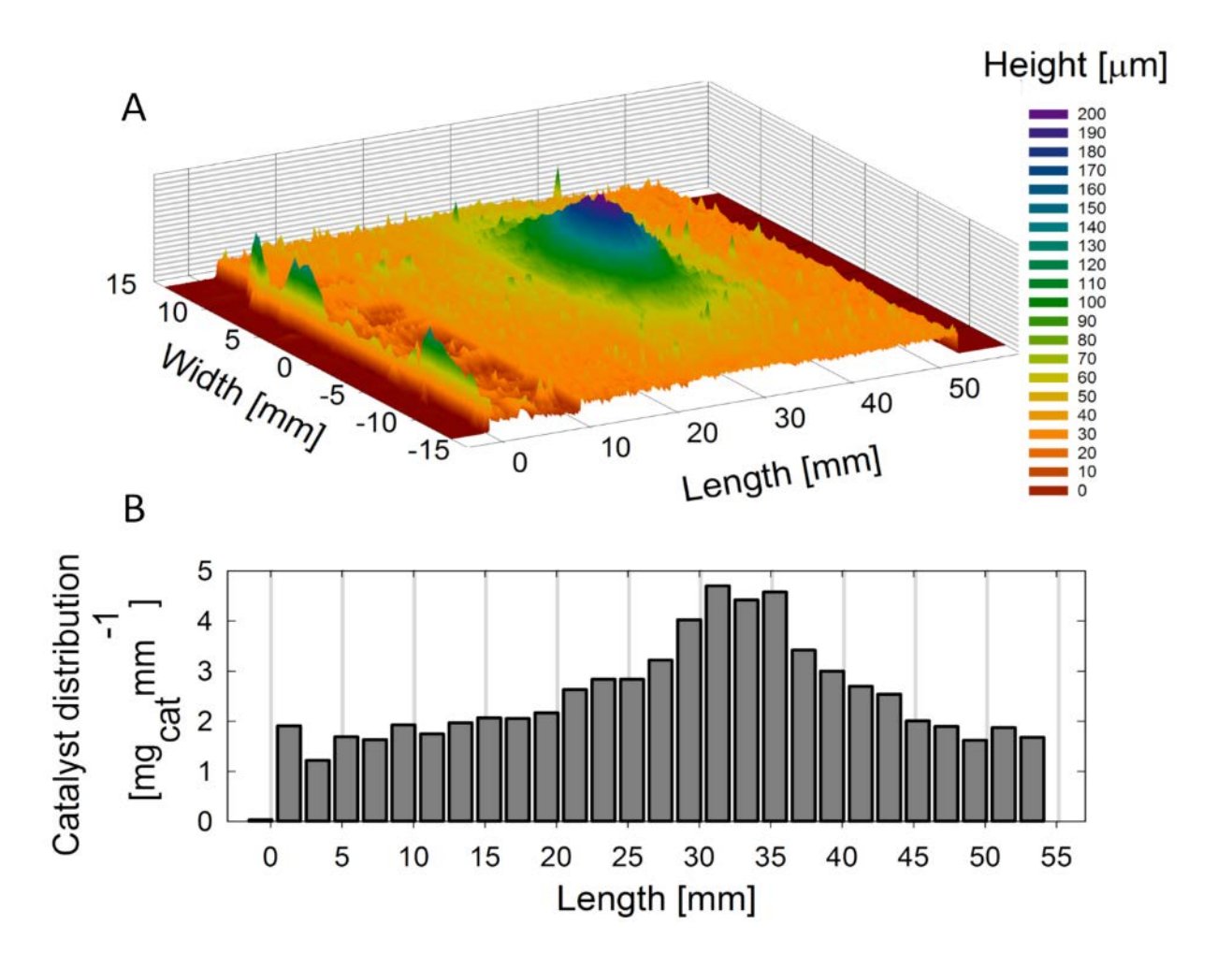


Figure 8

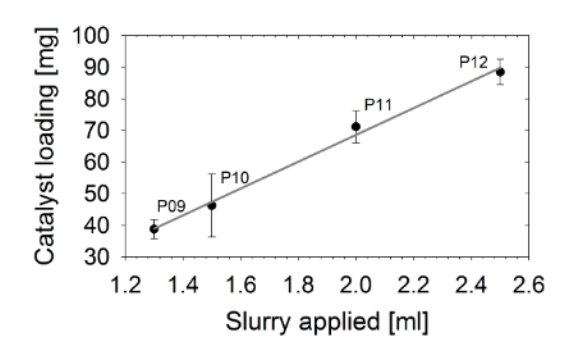
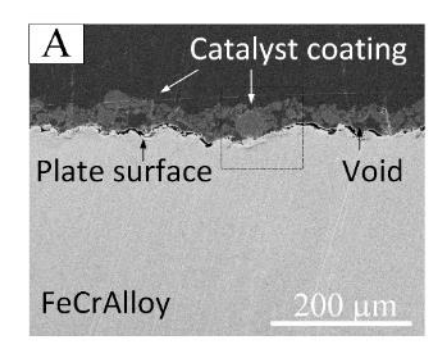
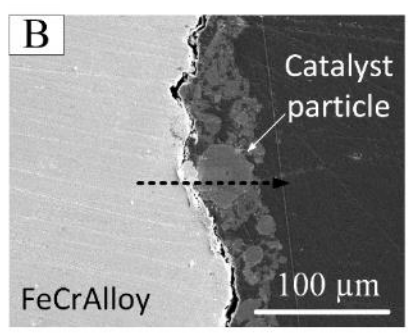


Figure 9





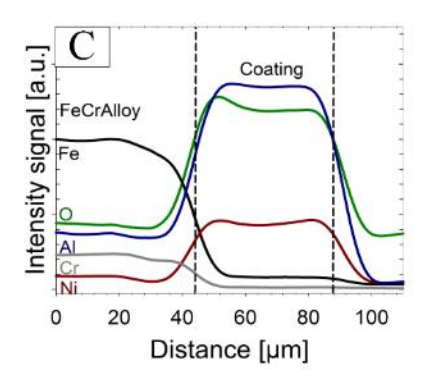


Figure 10

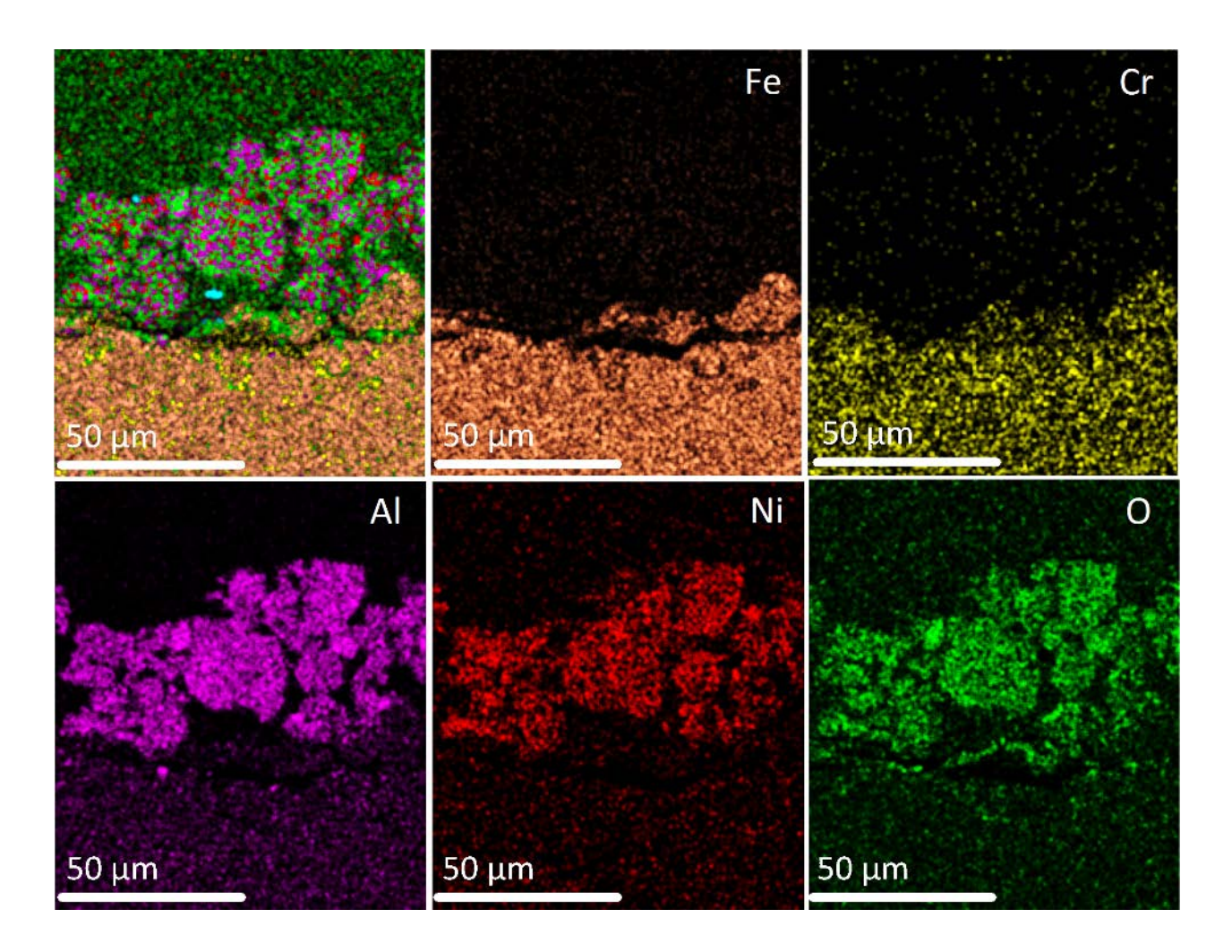


Figure 11

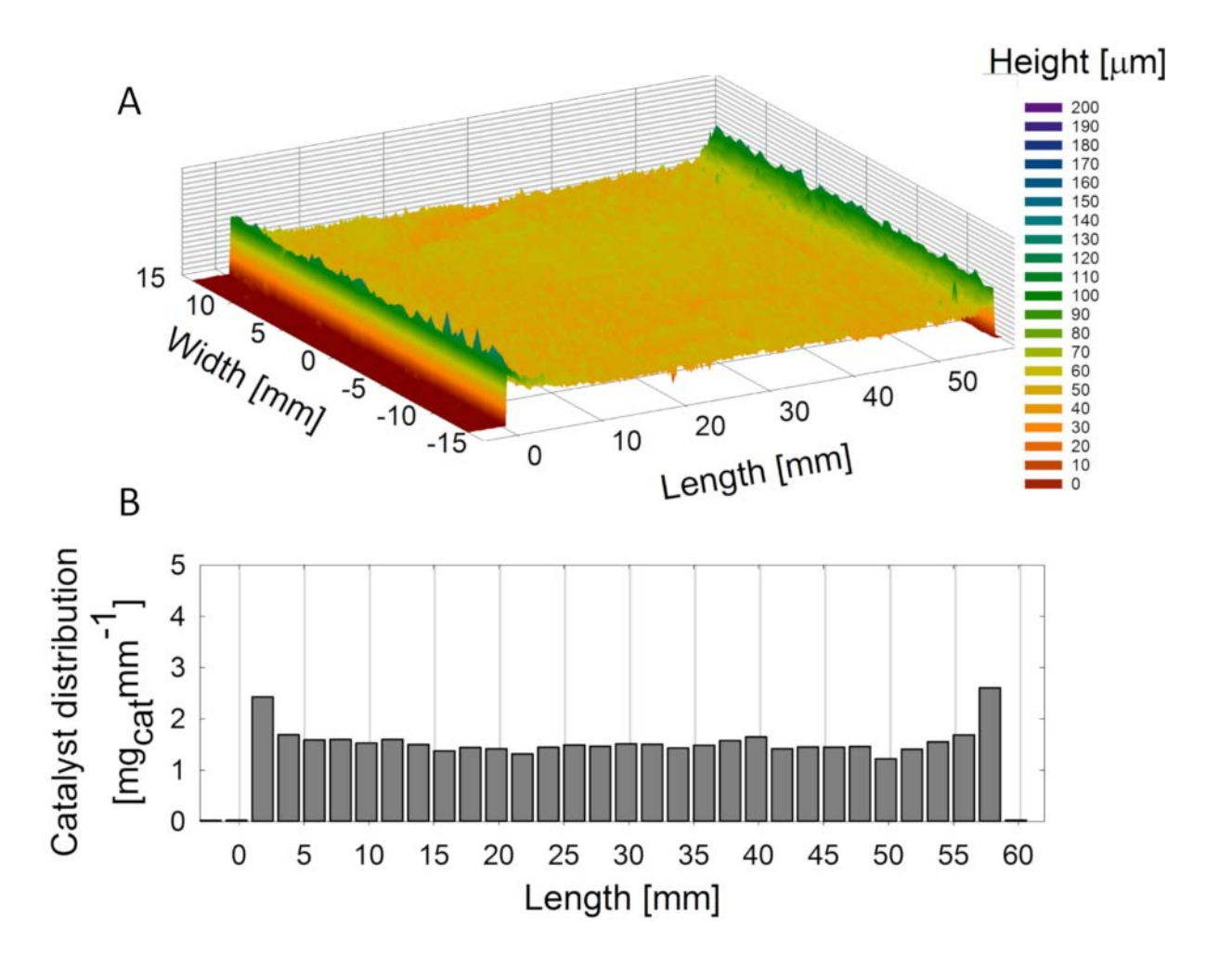


Figure 12

https://doi.org/10.1016/j.cej.2018.09.161

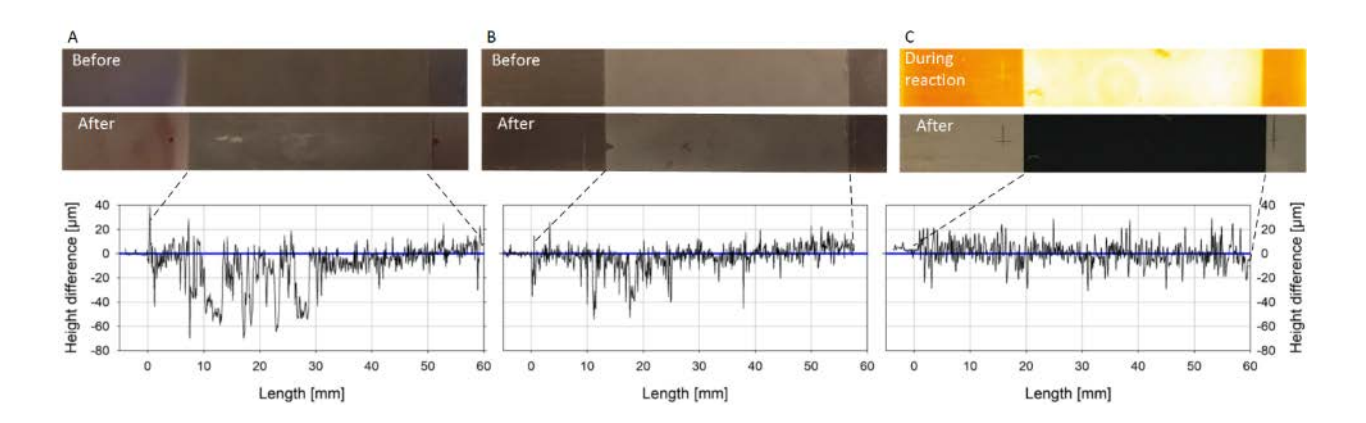


Figure 13

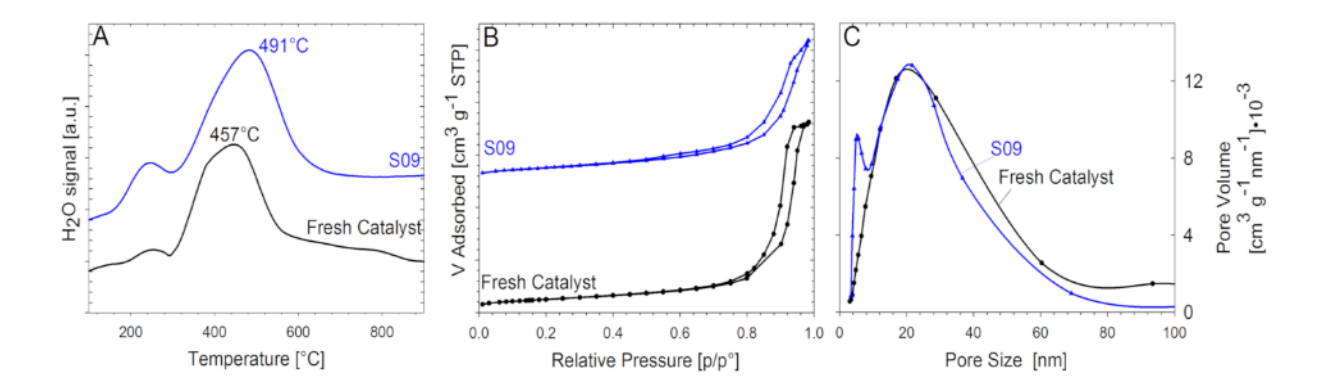


Figure 14

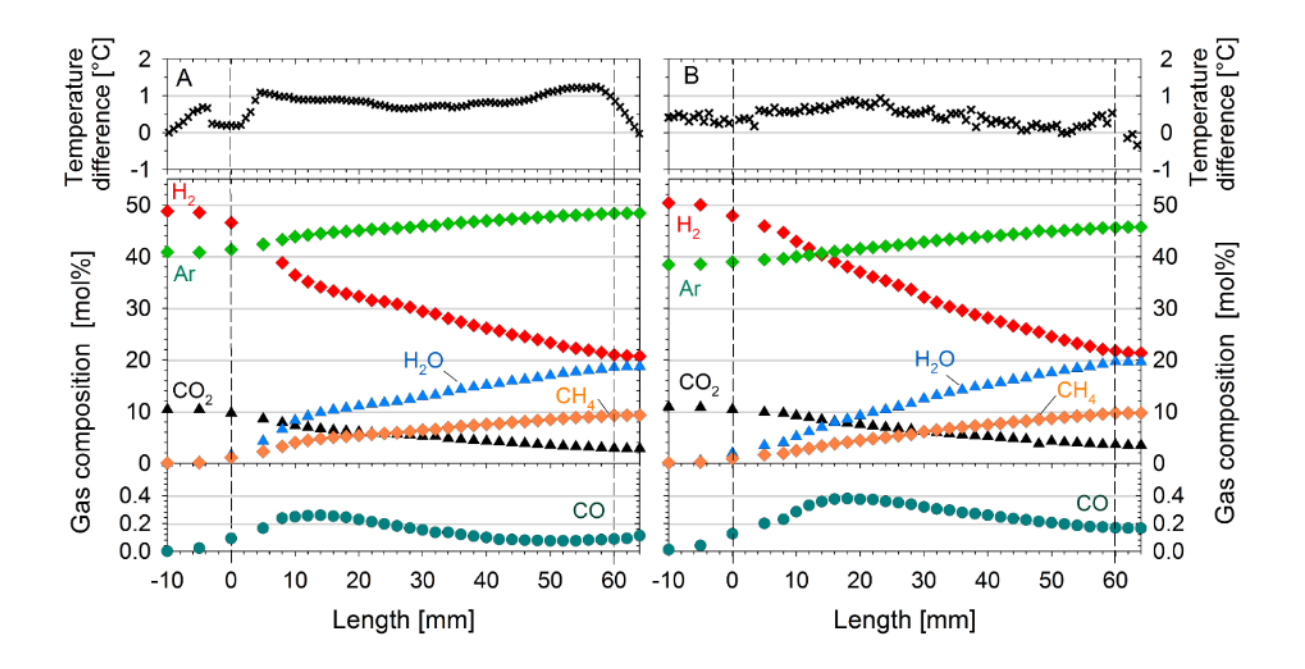


Figure 15

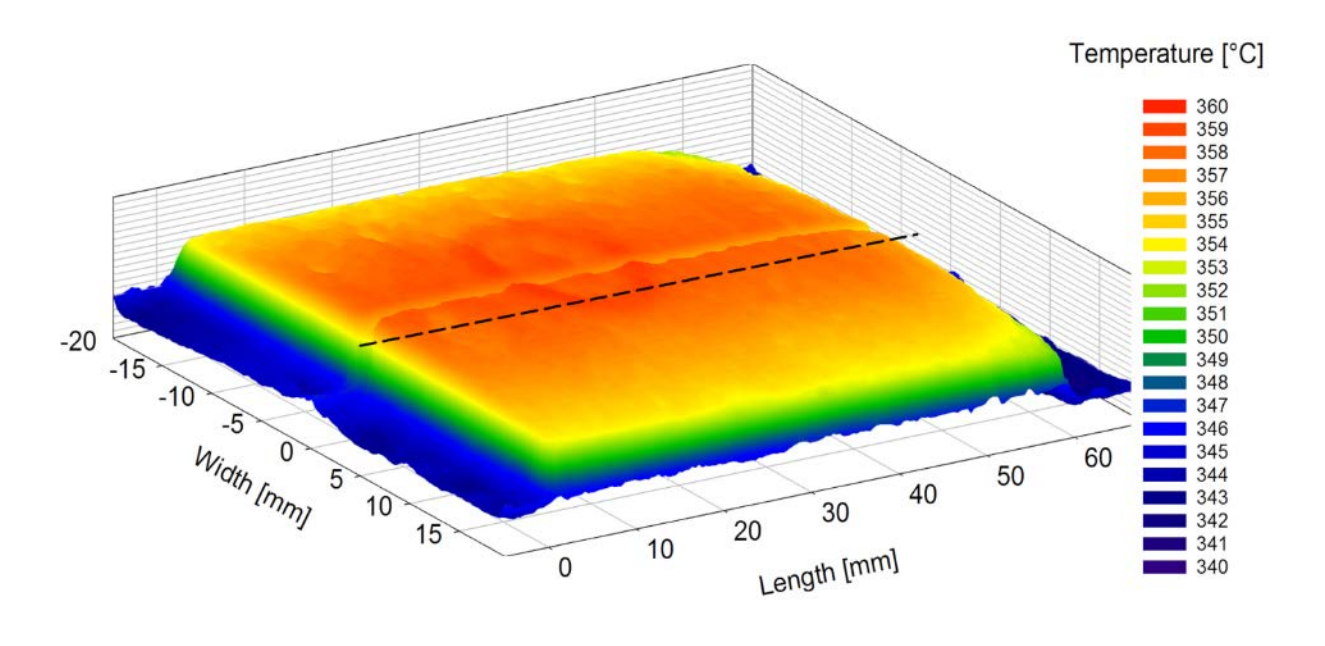


Figure 16